Materials Advances

ROYAL SOCIETY OF CHEMISTRY

PAPER

View Article Online
View Journal | View Issue

Cite this: *Mater. Adv.*, 2021, 2, 5712

Nanometer-thick [$(FPEA)_2PbX_4$; X = I and Br] 2D halide perovskite based thin films for pollutant detection and nonconventional photocatalytic degradation†

Arindam Mondal, Akash Lata, Aarya Prabhakaran and Satyajit Gupta *

Application of three-dimensional (3D)-halide perovskites (HaPs) in photocatalysis encourages the new exercise with two-dimensional (2D) HaP based thin-films for photocatalytic degradation of dyes. The reduced dimensionality to 2D-HaPs, with a structural formula of R_2PbX_4; R= organic spacer containing long chain amine and X = halide, offers better stability compared to 3D-HaPs. In this study, the potential of 2D-HaP thin-films towards the visible light-driven photocatalytic degradation of 2-mercaptobenzothiazole (MBT) was examined in hexane medium. The photo-physical properties of the 2D-HaPs were investigated as a function of 'X' site and their stability under ambient conditions was monitored. Thermal stability of the synthesized 2D-HaP thin-films was also examined by thermogravimetric analysis (TGA), which was found to be stable up to 250 °C. During the photocatalysis experiment, the rate constants of the thin-films were calculated to be 3–6 × 10^{-2} min^{-1}, under visible light illumination. Furthermore, cycling experiments were performed with the thin-films to understand their behaviour under repeated runs. Faster rate kinetics was observed when the 2D-HaP layer was coated over the titanium dioxide (TiO_2), indicating hole injection from the 2D-HaP thin-film surface to MBT. The adsorption of MBT over the 2D-HaP was also 'detected' using photoluminescence (PL) analysis. Thus, it revealed a promising photocatalytic behaviour of these 2D-HaP thin-films bringing a possibility of simultaneous 'detection and degradation' of toxic pollutants.

Received 27th June 2021,
Accepted 26th July 2021

DOI: 10.1039/d1ma00561h

rsc.li/materials-advances

Introduction

Three dimensional (3D) lead based halide perovskite (HaP) semiconductors [having a common structure of $APbX_3$ (where A = monovalent cation such as methyl ammonium (MA)/cesium (Cs^+); X = halide species such as chloride-Cl^-/bromide-Br^-/iodide-I^-] have drawn great scientific attention in recent years due to their low processing costs, high absorption co-efficient, large diffusion length, low exciton binding energy and tunable optoelectronic properties.[1–9] Perhaps, 3D-HaPs exhibit higher absorbing power of photons, offering an outstanding potential for photovoltaics.[10,11] Recently some specific compositions of lead (Pb^{2+}) based 3D-HaP revealed a high power conversion efficiency (PCE) up to >25%.[12–14] These quintessential 3D-HaPs have attracted immense interest of the scientific community to move forward to a new era with HaP-solar cells, light emitting diodes (LEDs), and photodetectors.[15,16] Widespread application of halide perovskites (HaPs) has been recently emphasized towards photocatalytic hydrogen generation, carbon dioxide reduction, and dye degradation.[17–24] However, (3D) AMX_3 based systems exhibit poor stability in the presence of moisture,[25–29] hindering their long-term applications. On the other hand, changing the dimensionality to two-dimensional (2D) HaP (with a structural formula of R_2PbX_4; R = long alkyl chain containing amines or aromatic ring substituted amines; X = halide species), it renders better stability than 3D-HaP with compromised performance.[30–33] 2D R_2PbX_4 comprises inorganic HaP layers (n = 1) of corner-sharing $[PbX_6]^{4-}$ octahedra, confined between interconnecting bilayers of long chain amine (either alkyl containing or aromatic ring substituted) cations. The 2D-HaP exhibits a 'quantum confinement effect' due to the formation of a quantum well, where inorganic layers are separated by the 'R group' as a spacer.[34,35] These 2D-HaP based thin films having suitable optoelectronic properties can play a major role in the photocatalytic degradation of toxic pollutants.

Department of Chemistry, IIT Bhilai, Raipur, Chhattisgarh, 492015, India.
E-mail: satyajit@iitbhilai.ac.in

† Electronic supplementary information (ESI) available: Tauc plot analysis, optical images of the films, absorbance of MBT as a function of time under UV-visible illumination, XRD and SEM images of the films (before and after photocatalysis), C/C_0 as a function of time, XRD analysis of $(FPEA)_2PbI_2Br_2$ after 1 month, the transmittance (%) as a function of wavelength for $(FPEA)_2PbI_2Br_2$ for day 1 and day 30, HPLC analysis, PL analysis of the films under illumination, table containing rate constants, and possible degradation mechanism. See DOI: 10.1039/d1ma00561h

There are a few reported literature studies on 3D-HaP based quantum-dots for photocatalytic degradation of dyes; however, to the best of our knowledge, 2D-HaP based thin-films for photocatalysis application have not been reported so far. In the case of photocatalysis using nanoparticles in dispersed form, the separation of nanoparticles is difficult (after the photocatalysis) as it needs centrifugation to separate them from the dispersion. This makes the process difficult and time consuming. However, in the case of thin-film based systems, the separation of the catalyst films over glass substrates becomes easier. In a photocatalytic reaction, after the light illumination, photo-generated electron–hole pairs diffuse at the surface of the semiconductor and participate in the 'red-ox' reaction. Herein, we have synthesized nanometer thick thin-films of 2D-HaP [R_2PbX_4; where R = 4-fluorophenethylammonium ($FC_6H_4(CH_2)_2NH_3^+$), which is abbreviated as FPEA and X = I and Br] to (i) to understand their photophysical properties as a function of 'X' site, and (ii) afterwards their photocatalytic activities were studied through photocatalytic degradation of a model dye. It is worthy of mention that lead (Pb^{2+}) is a harmful and biotoxic element to the environment in soluble form. However, in the present study while performing the photocatalysis experiment, hexane and dichloromethane (DCM) have been used, which are anti-solvents to the 2D-HaP; thereby, the perovskites remain insoluble in such solvent systems. Understanding the photocatalytic behaviour of such systems has attracted general scientific interest. The structure of $(FPEA)_2PbX_4$ is shown in Scheme 1.

Fluorine containing amine was chosen to impart hydrophobicity to the resulting films. The photocatalytic activities of the 2D-HaPs [$(FPEA)_2PbBr_4$, $(FPEA)_2PbI_2Br_2$, and $(FPEA)_2PbI_4$)] were realized through degradation of a toxic, poorly biodegradable, and carcinogenic[36] organo-sulphur dye–2-mercaptobenzothiazole (MBT) (having absorbance maxima at 325 nm wavelength) under visible light irradiation. MBT is widely used in the processes of copper corrosion inhibition, bio-corrosion inhibition, as a vulcanization accelerator in rubber technology, deoxygenation of epoxides and alkyne preparation.[37–39] The 2D-HaP thin-films with various halide species in the 'X' site (X = Br, I and a mixture of Br and I) were synthesized (over a glass/FTO substrate) using an anti-solvent assisted 'one-step' spin-coating method followed by thermal annealing at 120 °C (Scheme 2).

Their optical properties, phase purity, and thermal stability were evaluated using UV-visible, photoluminescence (PL), X-ray diffraction (XRD), and thermogravimetric analysis (TGA). The optical properties of the thin-films were observed to be strongly dependent on the nature of the halide species (X-site) and composition. The 2D-HaPs were found to be stable under ambient conditions and in hexane/DCM (during photocatalysis). Furthermore, photo(electro)chemical study provided more insights into the role of photogenerated 'charge-carriers' in the photocatalytic degradation of the dye.

Materials and methods

Materials

4-Fluorophenethylamine (99%), hydrobromic acid (48%), hydroiodic acid (57 wt% in water, 99.95%), lead bromide (99.999%), lead

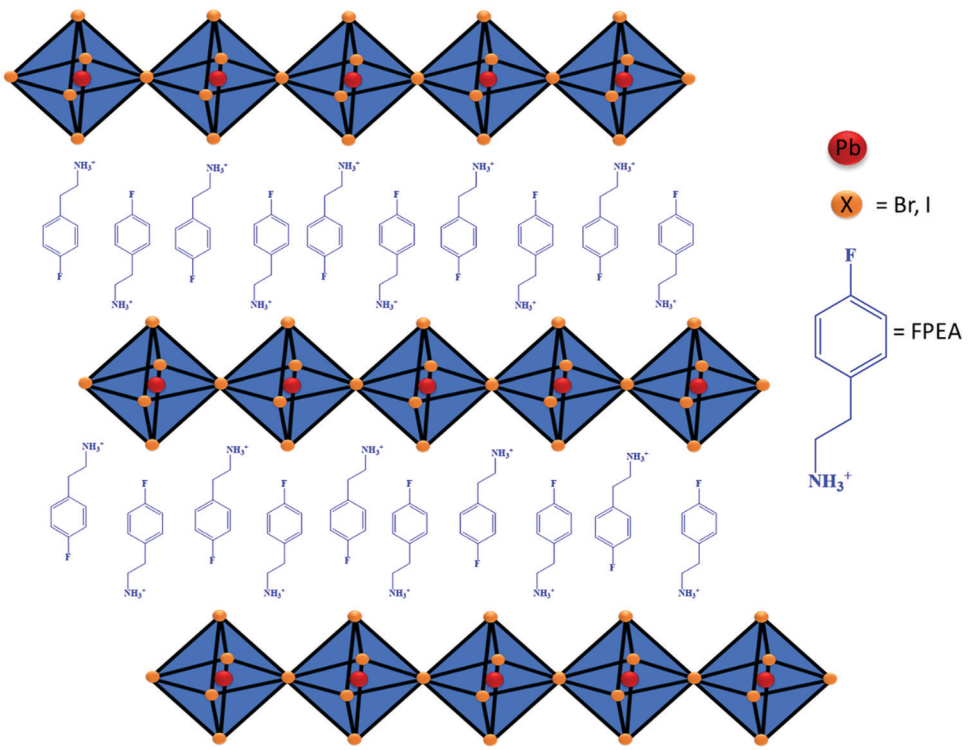

Scheme 1 Schematic representation of 2D-HaP–$(FPEA)_2PbX_4$.

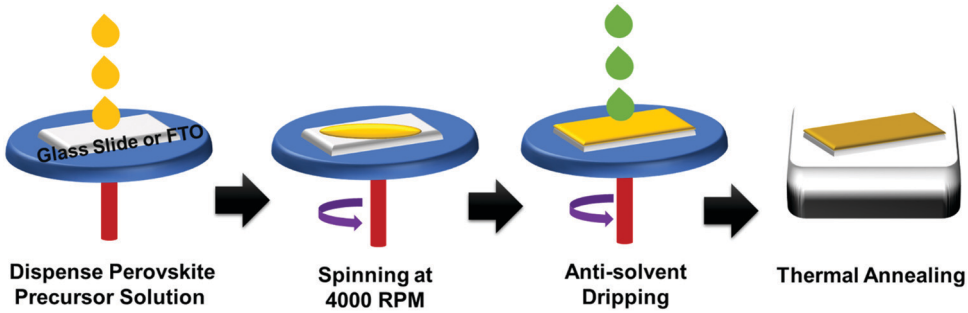

Scheme 2 Schematic of the fabrication of 2D-HaP thin-films through an anti-solvent (toluene) assisted 'one-step' spin-coating method followed by thermal annealing.

iodide (99%), dimethylformamide (99.8%), dimethyl sulfoxide (≥99.9%), dichloromethane (anhydrous, ≥99.8%), toluene (99.8%), hypophosphorous acid (50 wt% in water), hexene (≥97%), 2-mercaptobenzothiazole (97%), tetrabutylammonium hexafluorophosphate (98%), titanium(IV) isopropoxide (97%), and diethanol amine (≥98%) were procured from Sigma-Aldrich. AR grade ethanol, acetone, α-terpenol, ethyl cellulose, acetic acid, and diethyl ether were obtained from a local supplier. Aeroxide P25 TiO_2 was supplied by Evonik. Fluorinated Tin Oxide (FTO) coated glass (10–15 ohm sq^{-1}; transmittance >85% at 550 nm) was procured from Feeniks Technologies, India.

Synthesis of compact TiO_2 (c-TiO_2) over a glass or FTO substrate

The c-TiO_2 layer was coated over an FTO substrate by spin-coating of an ethanol solution containing titanium isopropoxide and diethanolamine and by annealing at 500 °C for 2 h.[40]

Synthesis of mesoporous TiO_2 (m-TiO_2) over c-TiO_2

1.2 g of P25 TiO_2, acetic acid, water, and ethanol were first mixed in a mortar-pestle. α-Terpenol, ethyl cellulose and ethanol were further added to it and mixed to form a homogeneous dispersion. The excess ethanol was evaporated to obtain a thick white paste.[41] The thick paste was diluted with ethanol and sonicated for 30 min. It was then spin-coated at 2000 rpm for 30 s twice and further annealing was carried out at 500 °C for 2 h.

Synthesis of 4-$FC_6H_4(CH_2)_2NH_3^+Br^-$ salt

$FC_6H_4(CH_2)_2NH_3^+Br^-$ salt was synthesized by drop-wise addition of aqueous hydrobromic acid (HBr) into an ethanolic solution of *p*-$FC_6H_4(CH_2)_2NH_2$ in 1 : 1 ratio under ice-cold conditions and the solution was continuously stirred for 2 h. Before starting the round bottom flask was filled with cold ethanol and during the synthesis, 3–4 drops of hypophosphorous acid (H_3PO_2) were added. After the reaction, a white-coloured precipitate was obtained. The precipitate was filtered and washed several times with diethyl ether and finally, it was filtered. The filtered precipitate was left overnight for drying at 45 °C in a vacuum oven and then it was used for further experiments.

Synthesis of 4-$FC_6H_4(CH_2)_2NH_3^+I^-$ salt

$FC_6H_4(CH_2)_2NH_3^+I^-$ salt was synthesized by drop-wise addition of aqueous hydroiodic acid (HI) into *p*-$FC_6H_4(CH_2)_2NH_2$ in 1 : 1 ratio under ice-cold conditions and continuously stirring for 2 h. Before starting the round bottom flask was filled with cold ethanol and during the synthesis 3–4 drops of H_3PO_2 were added. After the reaction, a white-coloured precipitate was obtained. The precipitate was washed several times with diethyl ether and finally, it was filtered. The filtered precipitate was left overnight for drying at 45 °C in a vacuum oven and then it was used for further experiments.

Preparation of thin films of 2D-HaPs

Glass slides and FTO slides were cut into 2 × 2 cm^2, then cleaned sequentially with soap solution and de-ionized (DI) water, and then sonicated in DI water, ethanol, and acetone for 10 min each followed by 15 min of UV-ozone treatment. The slides were dried and left for heating for 5 min at 80 °C on a hot plate.

The precursor salt solution containing (FPEA)X and PbX_2 (X = I and Br) was mixed in 2 : 1 ratio and taken into a glass vial so that the final ratio becomes 1 M. 1 mL of dimethylformamide (DMF)/dimethyl sulfoxide (DMSO) based mixed solvent in 4 : 1 ratio was added to the salt mixture. The mixture was dissolved using a vortex mixer at room temperature and stirred for 1 h to obtain a clear solution. All the fabrication processes were carried out under ambient conditions [relative humidity (%RH) of ~65–70% and 30 °C temperature].

Thin-film fabrication was carried out using the spin coating (Model: EZspin-A1 Apex Spin Coater) method. The process started with the dripping of 200 μL of precursor solution using a micropipette over the preheated glass-slide and FTO/c-TiO_2/m-TiO_2 *via* a one-step spin coating process; they were spin-coated at 4000 rpm for 20 s, and while at 17 s during the spinning, 500 μL of toluene (as anti-solvent) was dripped over the glass–substrate. After spin coating, the slides were directly transferred onto the hot plate and annealed at 120 °C temperature for 10 min to obtain the homogeneous HaP films.

Material characterization

Transmission spectra of films were measured using a UV-2600i spectrophotometer with an integrating sphere. Thermogravimetric analysis was performed on a Tarsus TG209 F3 by peeling off the coated HaP powder sample from thin films and at 30 °C–800 °C the crucible was heated. The precursor materials

(FPEA)Br and PbI_2 were also studied under the same experimental conditions. Photoluminescence spectra of the thin films (over glass) were collected using a Fluorolog FL3-211 HORIBA Scientific with a 450 watt Xenon arc lamp. Grazing incidence diffraction (GID) was performed for the thin films in a Bruker D8 Advance X-ray Diffractometer equipped with a Cu X-ray tube (40 kV and 40 mA). An Ultra55 FE-SEM (equipped with a Carl Zeiss EDS) was used to study the surface morphology and elemental composition of the thin-films. A Zeiss Gemini SEM500 was used for the study of thickness of thin-films. Films were coated with a thin layer of gold (Au) prior to SEM analysis. High performance liquid chromatography (HPLC) analysis was performed using a Shimadzu LC-2030C 3D Plus equipped with an auto-sampler and PDA detector, using an Inertsil SIL-100A 5 μm column (4.6 I.D. × 250 mm). The injection volume for the sample was 10 μL. The mobile phase was 5% isopropanol/hexane, and the flow rate was 1 mL min^{-1}. Chronoamperometric analysis was carried out using an electrochemical analyzer Metrohm Dropsens μStat-i 400s. A solar simulator from ScienceTech SciSun-150-C was used as a light source for the photoelectrochemistry experiment. A three-electrode system was used to analyze the photoelectrochemical behaviour of photoelectrodes [FTO/d-TiO_2/m-TiO_2/$(FPEA)_2PbX_4$, where X = Br and I] using platinum as the cathode and Ag/AgCl as the reference electrode and 100 mM tetrabutylammonium hexafluorophosphate ($^tBu_4NPF_6$) in dichloromethane was used as a supporting electrolyte.

Results and discussion

XRD was used to examine the phase purity and crystallinity of the $(FPEA)_2PbBr_4$, $(FPEA)_2PbI_2Br_2$, and $(FPEA)_2PbI_4$ based 2D-HaP thin-films over a glass-substrate. Fig. 1A illustrates sharp diffraction patterns of the materials with highly ordered peaks, which are distributed periodically, corresponding to 00*l* lattice planes.[41] Periodical peaks in the XRD suggest the layered structure of the synthesized 2D perovskites and presence of higher order peaks indicates well crystallized nature of the perovskite films.[42] The long-chain organic cation –FPEA, having a 'phenyl ring' can form bilayers through π–π interactions, providing the 2D perovskite with a periodic and layered crystal structure.[41] The thin-films exhibited pronounced peaks at a diffraction angle of = 5.1°, 10.2°, 15.3°, and 20.4° which can be indexed to (002), (004), (006), and (008) planes,[43,44] showing preferred orientation along 001 directions, which is in good agreement with earlier reported literature on 2D halide perovskites.[45]

Transmittance spectra of the samples are shown in Fig. 1B. As observed from the figure, a red-shift in the onset of the absorbance was observed with the increase in iodide content. The Tauc plot analysis (Fig. S1, ESI†) reflected a direct band-gap nature of the samples and the band-gaps were estimated from there. The band-gaps for $(FPEA)_2PbBr_4$, $(FPEA)_2PbI_2Br_2$, and $(FPEA)_2PbI_4$ were found to be 2.94 eV, 2.58 eV, and 2.33 eV respectively. Photoluminescence (PL) spectra of the samples are

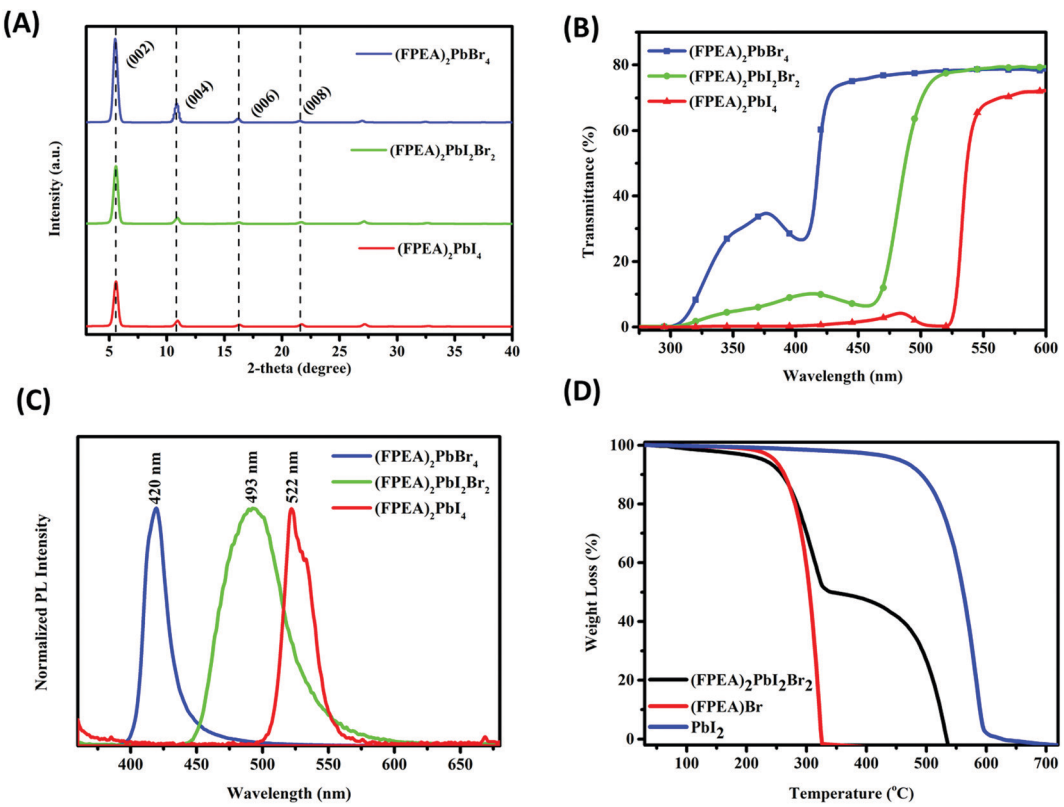

Fig. 1 (A) XRD pattern of the 2D-HaPs, showing sharp peaks, (B) transmittance spectra as a function of wavelength, and (C) normalized PL spectra of the 2D-HaP films as a function of 'X' site over glass. (D) TGA of $(FPEA)_2PbI_2Br_2$ showing thermal stability of the material up to 250 °C.

shown in Fig. 1C, which shows that $(FPEA)_2PbBr_4$, $(FPEA)_2PbI_2Br_2$, and $(FPEA)_2PbI_4$ exhibit emission wavelengths at 420, 493, and 522 nm respectively. The red-shift in PL emission with increasing iodide content is in agreement with the UV-visible analysis. The wider half peak width of $(FPEA)_2PbI_2Br_2$ compared to $(FPEA)_2PbBr_4$ and $(FPEA)_2PbI_4$ can be attributed to the compositional inhomogeneity in the $(FPEA)_2PbI_2Br_2$ having mixed halides in the 'X' site.[46] Furthermore, the exciton binding energies[47,48] were calculated from the difference between the band-gap and PL emission for the materials. The exciton binding energies were found to be 1 meV, 65 meV, and 45 meV for $(FPEA)_2PbBr_4$, $(FPEA)_2PbI_2Br_2$, and $(FPEA)_2PbI_4$ respectively, which resembles earlier reports.[49]

The thermal stability of the 2D-HaPs was examined using TGA. Weight loss (%) as a function of temperature for (FPEA)Br, PbI_2, and $(FPEA)_2PbI_2Br_2$ is shown in Fig. 1D, which indicates that the $(FPEA)_2PbI_2Br_2$ films are stable up to 250 °C. Furthermore, $(FPEA)_2PbI_2Br_2$ shows thermal degradation (Fig. 1D) in 'two-steps', originating from the precursor materials as (FPEA)Br and PbI_2 constitute 48% and 52% respectively of the total weight of the $(FPEA)_2PbI_2Br_2$. Thermal stability is an important criterion for an active layer for various real-time applications. Furthermore, ambient stability [relative humidity (%RH) of ~65–70% and 30 °C temperature] of the $(FPEA)_2PbI_2Br_2$ thin-films was tracked using transmittance measurements. No change in transmittance (Fig. S2A, ESI†) and XRD pattern (Fig. S2B, ESI†) was observed for a span of more than 1 month, indicating excellent stability of the materials.

The optical images of the thin-films are shown in Fig. S3 (ESI†). The surface morphology of the thin-films (with a thickness of 350 ± 25 nm; the cross-section of $(FPEA)_2PbI_2Br_2$ is shown in Fig. 2A) over the glass-substrate was examined using scanning electron microscopy analysis (as shown in Fig. 2B and C), which showed homogeneous deposition of 2D-HaP films over glass. The atomic percentage (%) of the various constituents (Pb, Br, and I) in the 2D-HaPs was analyzed using EDAX analysis and is shown in Table 1.

To understand the photocatalytic activity of the 2D-HaP films (coated over a glass substrate), a dye degradation experiment was performed using 0.06 mM solution of MBT (absorption maxima-λ_{max} = 325 nm) dissolved in hexane. The thin-films of 2D-HaPs were placed into a custom-made photoreactor, filled with the MBT solution, where the top-surface side of the films was placed towards the quartz window of the photoreactor. This was carried out under ambient conditions using a visible LED as the light source. Distance between the lamp source and the photoreactor was maintained as 10 cm throughout all the photocatalysis experiments (equivalent to 0.25 Sun; measured using a calibrated silicon photodiode). UV-Vis spectra of the solutions were measured in equal intervals of time during the course of the photocatalysis experiment to track the photocatalytic degradation of MBT.

Before the photocatalysis experiment, control experiments were performed using visible LED illumination on MBT solution in hexene (to examine light-mediated degradation/photolysis). No degradation of the dye was observed for a prolonged time, as indicated by the UV-visible absorbance measurement of the solution. However, when UV-visible light (using a solar simulator; AM1.5 illumination) was used for the dye solution (without the 2D-HaP films), significant degradation occurred for the dye due to photolysis (Fig. S4A, ESI†). Hence, during the photocatalysis experiment, visible-LED light was used for photocatalysis experiment to avoid any photolysis.

The synthesized 2D-HaP materials were observed to be efficient towards photocatalytic degradation of MBT. Photocatalysis

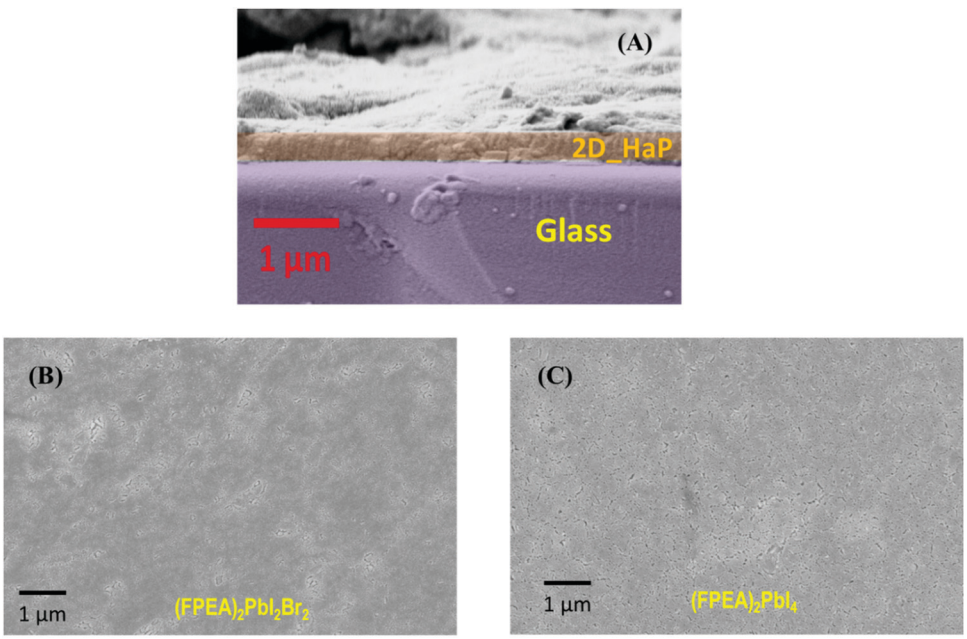

Fig. 2 (A) The cross-sectional SEM of the $(FPEA)_2PbI_2Br_2$ deposited over glass. SEM images of the surface of (B) $(FPEA)_2PbI_2Br_2$ and (C) $(FPEA)_2PbI_4$ deposited over glass.

Table 1 Elemental analysis of $(FPEA)_2PbBr_4$, $(FPEA)_2PbI_2Br_2$ and $(FPEA)_2PbI_4$ films, obtained from EDAX analysis

2D-HaP	Element	Atomic %
$(FPEA)_2PbBr_4$	Pb	16.76
	Br	74.24
$(FPEA)_2PbI_2Br_2$	Pb	11.13
	Br	36.98
	I	30.11
$(FPEA)_2PbI_4$	Pb	10.65
	I	49.33

experiments were carried out with $(FPEA)_2PbBr_4$, $(FPEA)_2PbI_2Br_2$, and $(FPEA)_2PbI_4$ thin-films over a glass substrate. The photocatalytic degradation was monitored through measuring the absorbance of the MBT solution as a function of time (Fig. 3A; the inset shows the chemical structure of MBT). It was observed that $(FPEA)_2PbBr_4$ did not show any degradation of dye under visible illumination which is due to its limited absorption at the visible wavelength, as indicated from the UV-visible absorption spectra (Fig. 1B) of $(FPEA)_2PbBr_4$ having a band-gap of 2.94 eV. Thus the photogenerated 'electron' and 'hole' pairs will be limited under visible light irradiation, resulting in no photocatalytic degradation of the dye. The UV-visible spectra of MBT solution as a function of time [during the photocatalytic experiment with $(FPEA)_2PbBr_4$] are shown in Fig S4B (ESI†). On the other hand, $(FPEA)_2PbBr_2I_2$ and $(FPEA)_2PbI_4$ showed significant photocatalytic activity under visible illumination.

From the kinetics study, as depicted in Fig. 3B, the '$\ln(C/C_0)$' of the dye decreased almost linearly as a function of irradiation time, which indicates 'pseudo-first-order' kinetics for the photocatalytic degradation of the dye. Here, (C/C_0) is the relative absorbance, where C_0 = initial absorbance of the dye and C = absorbance of the dye after illumination at a time interval of 15 minutes, measured at 325 nm wavelength. The rate constants were estimated from the slope of the linear fit of $\ln(C/C_0)$ as a function of time. The plot of (C/C_0) as a function of various 2D-HaPs is shown in Fig. S5 (ESI†). The degradation of MBT was observed to be completed upon continuous irradiation over a period of 75 minutes, as indicated by the UV-visible analysis. However, it was evident (in Fig. 3A) that after degradation, the absorbance peak at 273 nm is increasing with time. This reflects the formation of an intermediate organic compound from the degraded MBT. In order to understand if the photocatalytic degradation of MBT completes within 75 min, HPLC analysis of the MBT in hexane (before and after photocatalysis) was carried out. The characteristic peak of MBT appeared at T_R = 5.5 min (T_R = retention time) in the HPLC (Fig. S6A, ESI†). However, after photocatalysis, the peak at T_R = 5.5 was observed to completely disappear, while a new peak at T_R = 4.2 min rather appeared (Fig. S6B, ESI†), indicating that the degradation was completed. The new peak is due to the

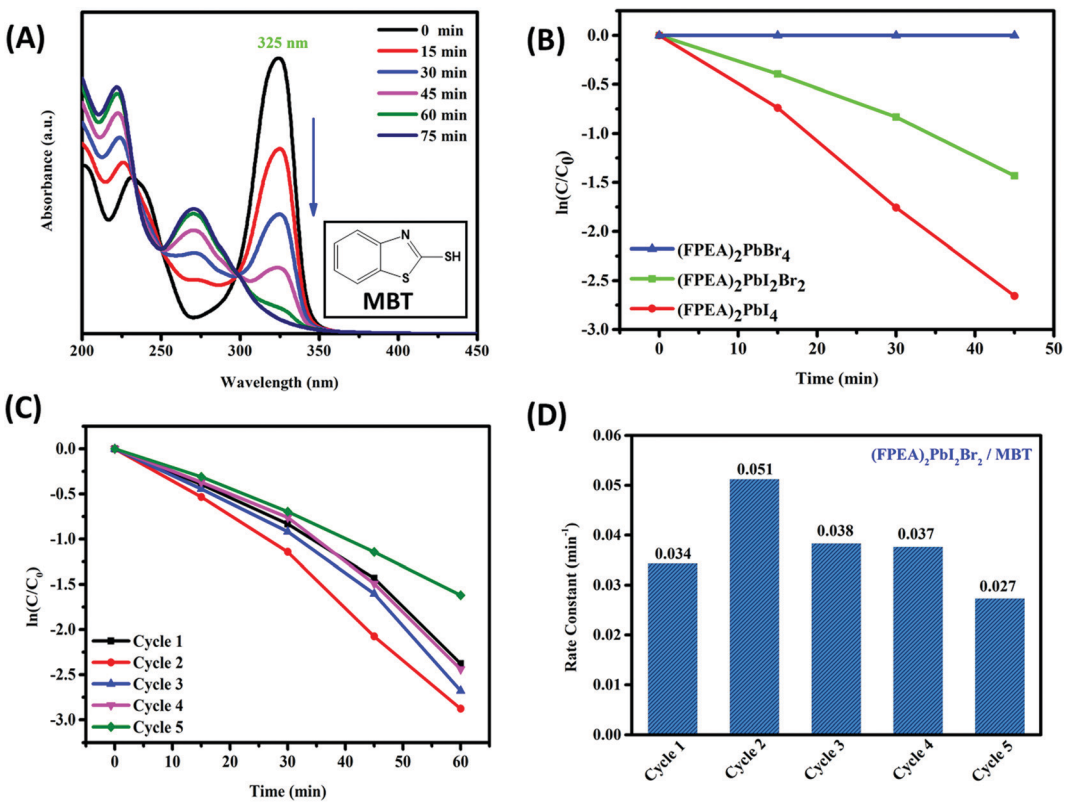

Fig. 3 (A) UV-Vis absorbance spectra of MBT as a function of time under visible light showing photocatalytic degradation in the presence of the $(FPEA)_2PbI_2Br_2$ thin-film. (B) $\ln(C/C_0)$ as a function of time for various 2D-HaPs. (c) $\ln(C/C_0)$ as a function of time of $(FPEA)_2PbI_2Br_2$ for 5 consecutive cycles during MBT degradation. (D) Rate constants of $(FPEA)_2PbI_2Br_2$ for 5 consecutive cycles.

degraded component of MBT (more details about the degraded product and possible mechanism are discussed later). It is important to mention that the 2D_HaP systems are unstable in water and thus they are not suitable for 'waste water treatment' in the current form. In this study, the photocatalysis was carried out in hexane medium (which is an anti-solvent to the 2D_HaP). In order to utilize such systems in water, the top surface and edges of the films need to be encapsulated using oxide-based solid state 'hole conductors' (such as nickel oxide – NiO) by the sputtering method. These 'hole conductors' may allow the photo-generated 'holes' from the '2D_HaPs' to react with the water soluble pollutants, while protecting the 2D_HaP thin-film from decomposition. In this case the active catalyst needs to be deposited over a conductive electrode such as FTO or indium tin oxide (ITO), coated with n-type oxides (such as TiO_2 or zinc oxide – ZnO) to channelize the photo-generated electrons. However, this is beyond the scope of the present study and worth further investigation.

The estimated rate constants for $(FPEA)_2PbI_2Br_2$ and $(FPEA)_2PbI_4$ were 0.034 min^{-1} and 0.06 min^{-1} respectively, which can be explained from the lower band-gap of $(FPEA)_2PbI_4$, compared to $(FPEA)_2PbI_2Br_2$, allowing for higher visible photon absorption and thus resulting in the generation of more electron–hole pairs. Moreover, the rate constants of the thin films were found to be much higher than those of previously reported $CsPbBr_3$ based nanoparticles (in slurry form; containing 0.08 mg ml^{-1} nanoparticles for photocatalysis), which showed a rate constant of 0.00302 min^{-1}.[19]

To understand the reusability of the thin films, a cycling experiment was performed with both $(FPEA)_2PbI_2Br_2$ and $(FPEA)_2PbI_4$ (Fig. 3C and Fig. S7A (ESI†) respectively show the $\ln(C/C_0)$ *vs.* time), immediately after each run. Surprisingly, it was observed that the photocatalytic activity was increased in the second cycle as evident from the sharp rise in rate constant up to ~49%, as compared to the same in first cycle (rate constant = 0.034 min^{-1}) for $(FPEA)_2PbI_2Br_2$, although the rate constant dropped after the second cycle (0.051 min^{-1}) and remained almost similar in the consecutive cycles (Fig. 3D). Similar behaviour was also observed with $(FPEA)_2PbI_4$, which showed an ~13% increase in the rate constant in the second cycle, compared to the first cycle (Fig. S7B, ESI†). The values of (C/C_0) as a function of time for 5 consecutive cycles of $(FPEA)_2PbI_2Br_2$ and $(FPEA)_2PbI_4$ during MBT degradation are shown in Fig. S8 and Fig. S9 respectively. The rate constant values of $(FPEA)_2PbI_2Br_2$ and $(FPEA)_2PbI_4$ are shown in Tables S1 and S2 respectively (ESI†).

The increase in the rate after the first cycle (Fig. 3C and D) is most likely due to photo mediated reduction in 'defect sites'[50,51] in the 2D-HaP thin-films, which improves the quality of the perovskite. To understand this behaviour, the film of $(FPEA)_2PbI_2Br_2$ was placed under continuous visible light illumination (using the same light source used for photocatalysis). The PL emission intensity from the samples was measured in an interval of 30 minutes. It was observed that PL emission intensity increased by ~9% until 1 h (as compared to freshly prepared films, t = 0; Fig. 4A-a), and remained almost constant, if illuminated further (Fig. 4A-c). After the continuous illumination (for 1 h; once PL emission intensity becomes constant), the films were placed in the dark (for 2 h) and the PL intensity of the films was observed to reduce and to return to its initial intensity (Fig. 4A-d), indicating reversibility of the process.[51] The increase in the magnitudes of PL emission values after constant illumination and further decrease are shown in Fig. 4B. Similar response was observed in $(FPEA)_2PbI_4$ (Fig. S10A and B, ESI†). Enhancement in PL emission intensity during light illumination signifies that enhanced radiative recombination of charge carriers is due to the reduction in the number of 'defect sites'. This improves the electronic quality of the 2D-HaP films.

After the second cycle of photocatalysis, a reduction in the rate constant was observed, which could be due to the adsorption of degraded components at the active sites of the thin-film surface, hindering the rate of photocatalysis in the next cycles. However, the possibility of degradation of the films after the second cycle cannot be ruled out. In order to understand if there is any degradation of the films after the 2nd and 5th cycles of photocatalysis, XRD and SEM of the films [both $(FPEA)_2PbI_2Br_2$

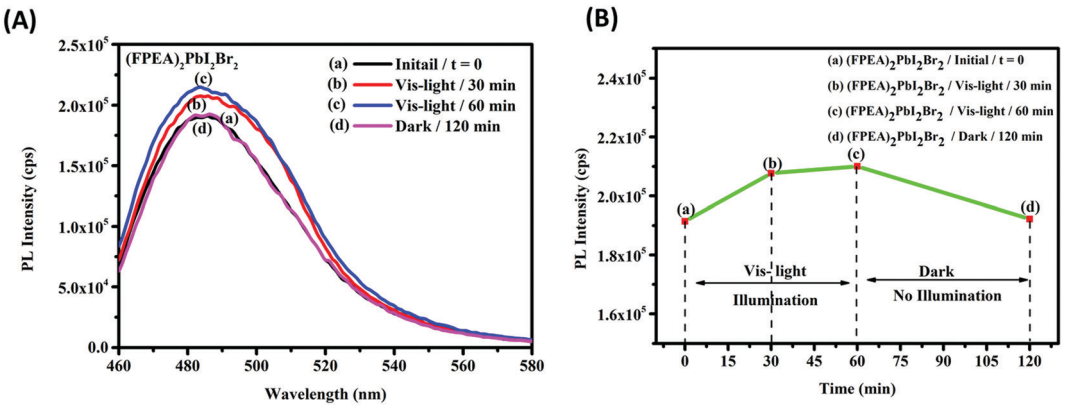

Fig. 4 (A) Increase in PL emission intensity for $(FPEA)_2PbI_2Br_2$ after constant visible light irradiation (b and c) compared to the initial PL emission intensity and then decrease in PL emission intensity (d) in the dark. (B) The increase in the corresponding magnitude of PL emission intensity values, followed by a decrease in the PL emission intensity value in the dark.

and $(FPEA)_2PbI_4$] were examined and compared to those of the fresh films. No change in the XRD pattern or, formation of additional peaks was observed after photocatalysis [Fig. S11 for $(FPEA)_2PbBr_2I_2$ ESI,† and Fig. 5 for $(FPEA)_2PbI_4$], which confirms that the material underwent no degradation after photocatalysis. Furthermore, SEM study also reveals that there was no change in the film morphology [Fig. S12 for $(FPEA)_2PbBr_2I_2$ and Fig. S13 for $(FPEA)_2PbI_4$; ESI†] after the 2nd and 5th cycles of photocatalysis, indicating that the photocatalysts were stable. Thus, it can be concluded that the decrease in the rate constant is due to adsorbed organic species at the surface, which blocks the active sites consequently.

The photocatalysis was also carried out under various light intensities. The intensity of visible light was adjusted by altering the distance (5, 10, and 15 cm) of the illumination source from the reactor. For $(FPEA)_2PbI_2Br_2$, $\ln(C/C_0)$ as a function of time for variation of the light intensity is shown in Fig. S14 (ESI†). C/C_0 values as a function of time are shown in Fig. S15 (ESI†). It can be noticed that light intensity does not alter the pseudo first-order kinetics. The reaction rate was found to be linearly dependent on the light intensity (Table S3; ESI†).

The photocatalytic activity of the 2D-HaP thin-film [$(FPEA)_2PbI_2Br_2$] was also evaluated over the c-TiO_2/m-TiO_2 coated glass surface using visible light illumination, for which a higher rate constant of 0.048 min^{-1} was observed, compared to bare glass (Fig. 6A; the inset shows the configuration of glass/c-TiO_2/m-TiO_2). This is due to TiO_2 being an n-type electron transporter, extracting photogenerated electrons and inhibiting the recombination process and thus the photogenerated holes at the surface are effectively responsible for photocatalytic degradation of MBT.

In order to gain more insights into the photocatalytic degradation of the dye, a photo(electro)chemistry[19] experiment was performed using FTO/c-TiO_2/m-TiO_2, deposited with $(FPEA)_2PbI_4$ and $(FPEA)_2PbI_2Br_2$ as photoanodes and Bu_4NPF_6 in dichloromethane (DCM) as the supporting electrolyte and under AM1.5 illumination using a solar simulator. To understand if the photocatalytic degradation process of the dye is electron mediated or hole mediated, chronoamperometry (under multiple on–off cycles) at zero applied bias (w.r.t. Ag/AgCl) was performed on the electrodes in (a) pure electrolyte (100 mM Bu_4NPF_6 in DCM) and, (b) MBT added electrolyte under both dark and light conditions. The results of the chronoamperometry are shown in Fig. 6B [$(FPEA)_2PbI_2Br_2$] and Fig. 6C [$(FPEA)_2PbI_4$]. In the absence of light, a very low current density was obtained for both $(FPEA)_2PbI_2Br_2$ and $(FPEA)_2PbI_4$ based photoanodes. However, under light illumination, a strong photo-response can be observed, because of the generation of electrons–hole pairs. The photo-generated electrons–hole pairs were separated and collected by their respective electrodes under fixed potentials (electrons were collected at the counter electrode and holes were injected onto the electrolyte solution). Interestingly, when MBT was added to the electrolyte solution, the photocurrent values from both $(FPEA)_2PbI_4$ and $(FPEA)_2PbI_2Br_2$ were observed to increase [31% for $(FPEA)_2PbI_4$, and 25% for $(FPEA)_2PbI_2Br_2$ – Fig. 6B and C respectively] compared to that of the pure electrolyte, indicating an efficient hole injection from the 2D-HaP surface to the MBT.

Photocatalytic oxidation of various 'organic thiols' using nanocrystals of $CsPbBr_3$ has been investigated earlier.[52] In the present study, it was observed from the UV-visible analysis of the photocatalytic degradation of MBT (Fig. 3A; discussed earlier) that the absorbance peak at 273 nm is increasing with time. The peak at 273 nm reflects the formation of a disulfide, 2,2′-dithiobis(benzothiazole)-MBTS, having a disulphide (S–S) bond.[53,54] This suggests that during photocatalysis, MBT molecules containing thiol (–SH) groups (the –SH group in 'aromatic thiols'/MBT is responsible for bio-toxicity[55,56]) oxidize to MBTS. Furthermore, our photo(electro)chemistry experiment (Fig. 6B and C) indicated that the 2D-HaP surface was responsible for efficient hole injection to the MBT molecules. Based on these observations, we propose a possible degradation mechanism of MBT in Fig. S16 (ESI†). First, the photogenerated holes are injected to the MBT molecules for the formation of MBT^+, which decomposes further to generate protons (H^+) and thiyl radicals, while the later couples to form MBTS. Since in the present study, the thin-film preparation and the photocatalysis experiments were carried out under ambient conditions, the dissolved oxygen in the 'hexane' is supposed to persist. Oxygen can react with photogenerated electrons to form super-oxide radicals [$^{\bullet}O_2^-$],[20] which may further react with H^+ to generate hydrogen peroxide (H_2O_2) and water (H_2O).[52]

The detection of the MBT molecules by the 2D-HaP thin-films was examined using PL analysis. The $(FPEA)_2PbI_2Br_2$ thin-films (over glass) were submerged into saturated MBT solution in dichloromethane (in the dark; for 30 min) and their PL emission intensity was verified both before and after dipping into MBT solution. It was observed that after dipping in DCM solution containing MBT, the PL emission intensity decreased drastically with a value of ~47% (Fig. 7A-b) compared to pristine $(FPEA)_2PbI_2Br_2$ (Fig. 7A-a). This phenomenon can be attributed to the adsorption of MBT molecules at the surface of the HaP films, extracting the charge carriers, and reducing the

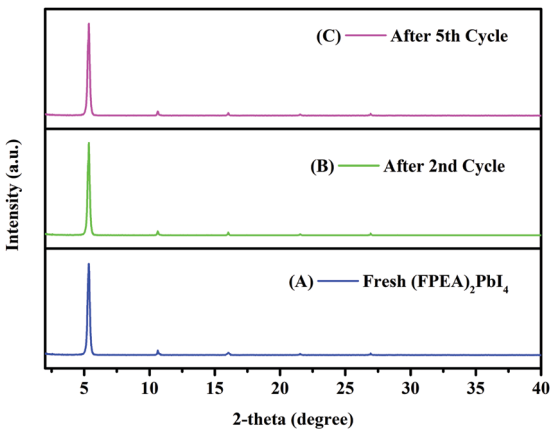

Fig. 5 XRD pattern of the fresh $(FPEA)_2PbI_4$ (A), after the 2nd cycle of photocatalysis (B), and after the 5th cycle of photocatalysis (C).

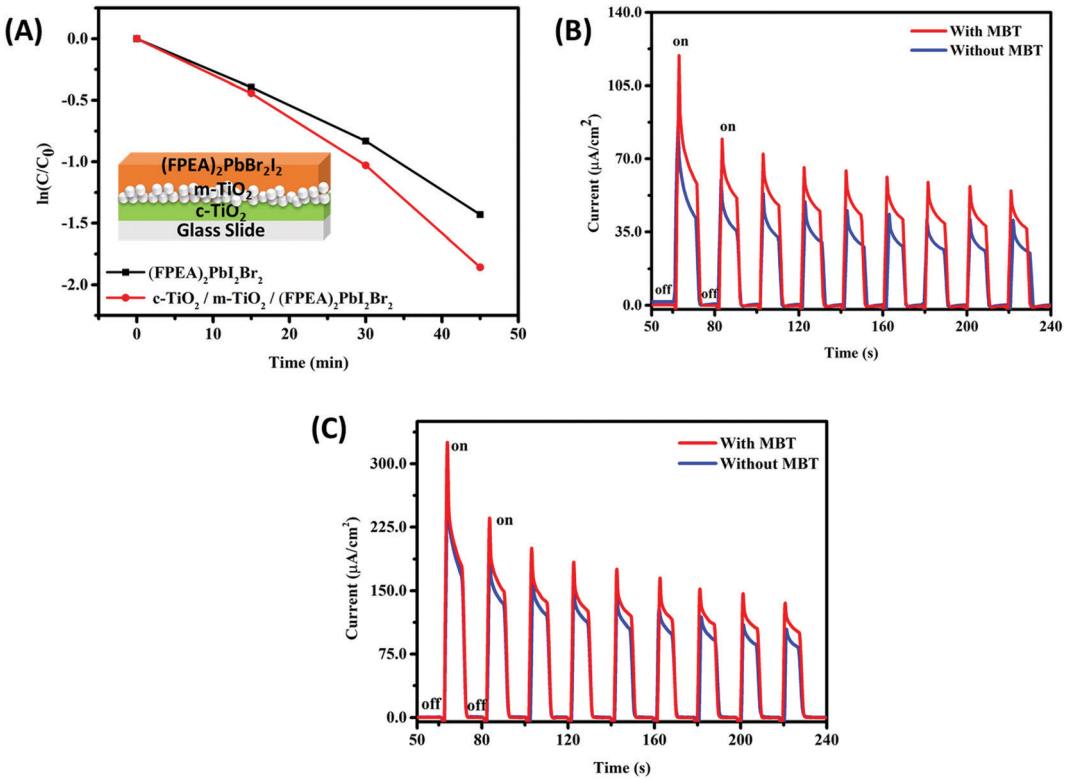

Fig. 6 (A) Comparison of $\ln(C/C_0)$ as a function of time between Glass/$(FPEA)_2PbI_2Br_2$ and glass/c-TiO_2/m-TiO_2/$(FPEA)_2PbI_2Br_2$ [figure A inset: the configuration used for glass/c-TiO_2/m-TiO_2/$(FPEA)_2PbI_2Br_2$], and chronoamperometric measurement of (B) FTO/c-TiO_2/m-TiO_2/$(FPEA)_2PbI_2Br_2$ and (C) FTO/c-TiO_2/m-TiO_2/$(FPEA)_2PbI_4$ films in 100 mM $^tBu_4NPF_6$ as the electrolyte in DCM, with and without MBT added to the electrolyte under chopped illumination.

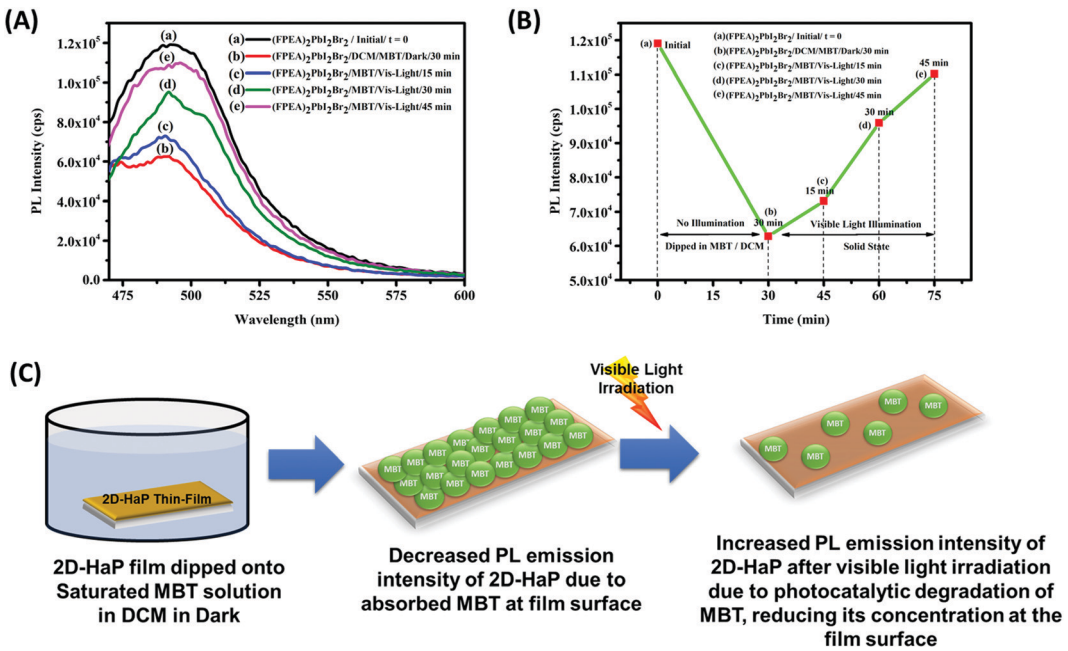

Fig. 7 (A) PL emission intensity of the $(FPEA)_2PbI_2Br_2$ film (a) before, and (b) after dipping into MBT solution in the dark, showing that MBT molecules are adsorbed at the surface. After illumination, an increase in PL intensity (c, d, and e) of the 2D-HaP as a function of time indicates the degradation of MBT in the solid-state. (B) The decrease in the magnitude of PL emission intensity values after dipping in the MBT solution in DCM and light mediated enhancement of PL intensity. (C) Schematic of the overall process occurring at the thin-film surface of the 2D-HaP in the solid-state.

PL emission intensity. Furthermore, when the films (adsorbed with MBT) were illuminated with visible light, the PL emission intensity was increased as a function of time [Fig. 7A: c-15 min of illumination, Fig. 7A: d-30 minutes of illumination, and Fig. 7A: e-45 minutes of illumination)], suggesting the degradation of the adsorbed MBT in the solid-state. The decrease in the PL emission intensity values after dipping into DCM solution containing MBT, followed by light mediated enhancement of PL emission intensity, is shown in Fig. 7B. This suggests that the toxic pollutant can be detected by the 2D-HaPs and can be degraded as well in the solid-state. A schematic of the process occurring at the surface is shown in Fig. 7C. The same experiment was also conducted for $(FPEA)_2PbI_4$, which showed the same behaviour as $(FPEA)_2PbI_2Br_2$ (Fig. S17; ESI†).

Conclusion

In summary, the optical properties of the various 2D-HaPs [$(FPEA)_2PbX_4$; X = Br, I and a mixture] were evaluated and the films were observed to be thermally stable. The band-gap and emission peak showed a 'red-shift' with an increase in the iodide content in the thin-film. The films were further used for the photocatalytic degradation of an organic dye MBT and proved themselves as excellent photocatalysts. The rate constant of photocatalysis was observed to increase after the first cycle, emphasizing the reusability of the films. Visible-light assisted reduction in 'defect sites' in the 2D-HaP thin-films was further studied. Moreover, photo(electro)chemical studies provided further insights into the hole injection into the dye. The study indicated that the use of 2D-HaP films can be feasible and efficient for detection and photocatalytic degradation of pollutants.

Conflicts of interest

There is no conflict to declare.

Acknowledgements

SG thanks SERB for the fellowship of AL and AP through the Start-up Research Grant (SRG/2019/000157). AM thanks MHRD for research fellowship. SG thanks IIT Bhilai for Research Initiation Grant. The authors thank Dr Ganapathy D. from the Department of Chemistry (IIT Bhilai) for helpful discussions on HPLC analysis and Mr Sandeep from IISc, Bangalore, for discussions on SEM analysis.

References

1 T. M. Brenner, D. A. Egger, L. Kronik, G. Hodes and D. Cahen, *Nat. Rev. Mater.*, 2016, **1**, 15007–15023.
2 M. A. Green, A. Ho-Baillie and H. J. Snaith, *Nat. Photonics*, 2014, **8**, 506–514.
3 N. J. Jeon, J. H. Noh, Y. C. Kim, W. S. Yang, S. Ryu and S. Il Seok, *Nat. Mater.*, 2014, **13**, 897–903.
4 Q. A. Akkerman, G. Rainò, M. V. Kovalenko and L. Manna, *Nat. Mater.*, 2018, **17**, 394–405.
5 M. D. Smith and H. I. Karunadasa, *Acc. Chem. Res.*, 2018, **51**, 619–627.
6 C. C. Stoumpos and M. G. Kanatzidis, *Adv. Mater.*, 2016, **28**, 5778–5793.
7 S. D. Stranks, G. E. Eperon, G. Grancini, C. Menelaou, M. J. P. Alcocer, T. Leijtens, L. M. Herz, A. Petrozza and H. J. Snaith, *Science*, 2013, **342**, 341–344.
8 P. S. Mathew, P. S. Mathew, G. F. Samu, G. F. Samu, C. Janáky, P. V. Kamat, P. V. Kamat and P. V. Kamat, *ACS Energy Lett.*, 2020, **5**, 1872–1880.
9 K. P. Goetz, A. D. Taylor, F. Paulus and Y. Vaynzof, *Adv. Funct. Mater.*, 2020, **30**, 1910004.
10 A. Sadhanala, S. Ahmad, B. Zhao, N. Giesbrecht, P. M. Pearce, F. Deschler, R. L. Z. Hoye, K. C. Gödel, T. Bein, P. Docampo, S. E. Dutton, M. F. L. De Volder and R. H. Friend, *Nano Lett.*, 2015, **15**, 6095–6101.
11 S. Tombe, G. Adam, H. Heilbrunner, D. H. Apaydin, C. Ulbricht, N. S. Sariciftci, C. J. Arendse, E. Iwuoha and M. C. Scharber, *J. Mater. Chem. C*, 2017, **5**, 1714–1723.
12 National Renewable Energy Laboratory, Best Research-Cell Efficiencies, 2020 https://www.nrel.gov/pv/assets/pdfs/pv-efficiencies-04-01-2020.pdf.
13 J. Y. Kim, J. W. Lee, H. S. Jung, H. Shin and N. G. Park, *Chem. Rev.*, 2020, **120**, 7867–7918.
14 M. A. Green, E. D. Dunlop, D. H. Levi, J. Hohl-Ebinger, M. Yoshita and A. W. Y. Ho-Baillie, *Prog. Photovoltaics*, 2019, **27**, 565–575.
15 C. Xie, C. K. Liu, H. L. Loi and F. Yan, *Adv. Funct. Mater.*, 2020, **30**, 1–28.
16 S. Heo, G. Seo, K. T. Cho, Y. Lee, S. Paek, S. Kim, M. Seol, S. H. Kim, D. J. Yun, K. Kim, J. Park, J. Lee, L. Lechner, T. Rodgers, J. W. Chung, J. S. Kim, D. Lee, S. H. Choi and M. K. Nazeeruddin, *Adv. Energy Mater.*, 2019, **9**, 1–8.
17 X. Liu, Y. Wang, X. Cui, M. Zhang, B. Wang, M. Rager, Z. Shu, Y. Yang, Z. Li and Z. Lin, *J. Mater. Chem. A*, 2019, **7**, 165–171.
18 S. Shyamal and N. Pradhan, *J. Phys. Chem. Lett.*, 2020, **11**, 6921–6934.
19 D. Cardenas-Morcoso, A. F. Gualdrón-Reyes, A. B. Ferreira Vitoreti, M. García-Tecedor, S. J. Yoon, M. Solis De La Fuente, I. Mora-Seró and S. Gimenez, *J. Phys. Chem. Lett.*, 2019, **10**, 630–636.
20 Z. Zhang, Y. Liang, H. Huang, X. Liu, Q. Li, L. Chen and D. Xu, *Angew. Chem., Int. Ed.*, 2019, **58**, 7263–7267.
21 G. F. Samu, R. A. Scheidt, P. V. Kamat and C. Janáky, *Chem. Mater.*, 2018, **30**, 561–569.
22 M. Wang, Y. Zuo, J. Wang, Y. Wang, X. Shen, B. Qiu, L. Cai, F. Zhou, S. P. Lau and Y. Chai, *Adv. Energy Mater.*, 2019, **9**, 1–7.
23 F. Liu, M. Wang, X. Liu, B. Wang, C. Li, C. Liu, Z. Lin and F. Huang, *Nano Lett.*, 2021, **21**, 1643–1650.
24 S. Park, W. J. Chang, C. W. Lee, S. Park, H. Y. Ahn and K. T. Nam, *Nat. Energy*, 2017, **2**, 1–8.
25 J. Yang, B. D. Siempelkamp, D. Liu and T. L. Kelly, *ACS Nano*, 2015, **9**, 1955–1963.
26 J. A. Christians, P. A. Miranda Herrera and P. V. Kamat, *J. Am. Chem. Soc.*, 2015, **137**, 1530–1538.

27 C. Peng, J. Chen, H. Wang and P. Hu, *J. Phys. Chem. C*, 2018, **122**, 27340–27349.
28 H. Xu, *IOP Conf. Ser. Earth Environ. Sci.*, 2020, **585**, 012027.
29 S. Lou, T. Xuan and J. Wang, *Opt. Mater. X*, 2019, **1**, 100023.
30 Y. Lekina and Z. X. Shen, *J. Sci. Adv. Mater. Devices*, 2019, **4**, 189–200.
31 R. Yang, R. Li, Y. Cao, Y. Wei, Y. Miao, W. L. Tan, X. Jiao, H. Chen, L. Zhang, Q. Chen, H. Zhang, W. Zou, Y. Wang, M. Yang, C. Yi, N. Wang, F. Gao, C. R. McNeill, T. Qin, J. Wang and W. Huang, *Adv. Mater.*, 2018, **30**, 1–8.
32 G. Liu, H. Zheng, X. Xu, S. Xu, X. Zhang, X. Pan and S. Dai, *Adv. Funct. Mater.*, 2019, **29**, 1–9.
33 S. Tian, J. Chen, X. Lian, Y. Wang, Y. Zhang, W. Yang, G. Wu, W. Qiu and H. Chen, *J. Mater. Chem. A*, 2019, **7**, 14027–14032.
34 S. Chen, N. Shen, L. Zhang, W. Kong, L. Zhang, C. Cheng and B. Xu, *J. Mater. Chem. A*, 2019, **7**, 9542–9549.
35 I. García-Benito, C. Quarti, V. I. E. Queloz, Y. J. Hofstetter, D. Becker-Koch, P. Caprioglio, D. Neher, S. Orlandi, M. Cavazzini, G. Pozzi, J. Even, M. K. Nazeeruddin, Y. Vaynzof and G. Grancini, *Front. Chem.*, 2020, **7**, 1–11.
36 T. Sorahan, *Occup. Environ. Med.*, 2009, **66**, 269–273.
37 F. Li, C. Liu, C. Liang, X. Li and L. Zhang, *J. Hazard. Mater.*, 2008, **154**, 1098–1105.
38 X. Liu, J. Ding, N. Ren, Q. Tong and L. Zhang, *Int. J. Environ. Res. Public Health*, 2016, **13**, 1259–1271.
39 M. Celeiro, D. Armada, T. Dagnac, J. de Boer and M. Llompart, *Sci. Total Environ.*, 2021, **755**, 142566.
40 J. Liang, C. Wang, Y. Wang, Z. Xu, Z. Lu, Y. Ma, H. Zhu, Y. Hu, C. Xiao, X. Yi, G. Zhu, H. Lv, L. Ma, T. Chen, Z. Tie, Z. Jin and J. Liu, *J. Am. Chem. Soc.*, 2016, **138**, 15829–15832.
41 Y. Hu, L. M. Spies, D. Alonso-Álvarez, P. Mocherla, H. Jones, J. Hanisch, T. Bein, P. R. F. Barnes and P. Docampo, *J. Mater. Chem. A*, 2018, **6**, 22215–22225.
42 Y. Zhang, Y. Liu, Z. Xu, H. Ye, Q. Li, M. Hu, Z. Yang and S. Liu, *J. Mater. Chem. C*, 2019, **7**, 1584–1591.
43 K. Liang, D. B. Mitzi and M. T. Prikas, *Chem. Mater.*, 1998, **10**, 403–411.
44 B. El Cohen, M. Wierzbowska and L. Etgar, *Sustainable Energy Fuels*, 2017, **1**, 1935–1943.
45 C. Liang, D. Zhao, Y. Li, X. Li, S. Peng, G. Shao and G. Xing, *Energy Environ. Mater.*, 2018, **1**, 221–231.
46 M. Karlsson, Z. Yi, S. Reichert, X. Luo, W. Lin, Z. Zhang, C. Bao, R. Zhang, S. Bai, G. Zheng, P. Teng, L. Duan, Y. Lu, K. Zheng, T. Pullerits, C. Deibel, W. Xu, R. Friend and F. Gao, *Nat. Commun.*, 2021, **12**, 1–10.
47 M. Kolos and F. Karlický, *Phys. Chem. Chem. Phys.*, 2019, **21**, 3999–4005.
48 J. L. Bredas, *Mater. Horiz.*, 2014, **1**, 17–19.
49 S. Sharifzadeh, A. Biller, L. Kronik and J. B. Neaton, *Phys. Rev. B: Condens. Matter Mater. Phys.*, 2012, **85**, 1–27.
50 Y. Tian, M. Peter, E. Unger, M. Abdellah, K. Zheng, T. Pullerits, A. Yartsev, V. Sundström and I. G. Scheblykin, *Phys. Chem. Chem. Phys.*, 2015, **17**, 24978–24987.
51 D. W. DeQuilettes, W. Zhang, V. M. Burlakov, D. J. Graham, T. Leijtens, A. Osherov, V. Bulović, H. J. Snaith, D. S. Ginger and S. D. Stranks, *Nat. Commun.*, 2016, **7**, 11683–11692.
52 W. B. Wu, Y. C. Wong, Z. K. Tan and J. Wu, *Catal. Sci. Technol.*, 2018, **8**, 4257–4263.
53 Z. Zajíčková and C. Párkányi, *J. Liq. Chromatogr. Relat. Technol.*, 2009, **32**, 1032–1043.
54 I. Chipinda, J. M. Hettick, R. H. Simoyi and P. D. Siegel, *Chem. Res. Toxicol.*, 2007, **20**, 1084–1092.
55 P. Amrolia, S. G. Sullivan, A. Stern and R. Munday, *J. Appl. Toxicol.*, 1989, **9**, 113–118.
56 I. Chipinda, X. D. Zhang, R. H. Simoyi and P. D. Siegel, *Cutan. Ocul. Toxicol.*, 2008, **27**, 103–116.